Analysis of the Effects of In-Cylinder Flows during Intake Stroke on the Flow Characteristics near Compression TDC in Four-Stroke Cycle Engines

T.Wakisaka, Y.Shimamoto, Y.Isshiki, N.Sumi, K.Tamura and R.M.Modien

Department of Mechanical Engineering
Kyoto University
Yoshida, Sakyo-ku
Kyoto 606
Japan

ABSTRACT

The purpose of this study is to reveal the effects of tumbling flow and inclined swirl on the turbulent flow characteristics near compression TDC in four-stroke cycle engines by numerically analyzing the in-cylinder flows using the $k-\varepsilon$ model.

By means of a new calculation method (the GTT method) based on the finite-volume method and body fitted non-orthogonal grids, three-dimensional air flows in the whole region of the intake port and cylinder, including the moving intake valve with a stem, have been successfully computed in single- and dual-intake valve engines.

In a single-intake valve engine, the variations of the tumble and swirl components at intake BDC with the configuration and orientation of intake port have been demonstrated. In dual-intake valve engines, it has been found that the tumbling flow generates much stronger turbulence near compression TDC in both disc-type and pentroof-type combustion chambers than does the solid-body swirl around the cylinder axis. It is inferred that the inclined swirl may be effective for promoting combustion in spark-ignition engines if its large kinetic energy near compression TDC could be converted into turbulence energy.

INTRODUCTION

In-cylinder flows including a vertical vortex component, i.e. tumbling flow and inclined swirl, are said to be effective for promoting combustion in spark ignition engines (1), (2); of course the effectiveness of ordinary horizontal swirl and squish flow are known. Recently, many studies on such tumble-related flows have been carried out experimentally (3), (4), (5) and numerically (3), (6), (7) because of their potential to enhance turbulence intensity near compression TDC.

The purpose of this study is to reveal the effects of induction-generated flows, especially tumbling flow and inclined swirl, on the turbulent flow characteristics near compression TDC in four-stroke cycle engines by means of numerical analysis. For this purpose, a new calculation method has been developed to compute the air flows in the whole region of the intake port/valve and cylinder.

Firstly, using this method, the effects of the configuration and orientation of intake port on the in-cylinder flow during intake stroke are examined in a single-intake valve engine. Secondly, by referring to these results, the velocity distributions around intake valves are prescribed in a dual-intake valve engine with a disk-type combustion chamber, and otherwise the intake port configurations are determined in a dual-intake valve engine with a pentroof-type combustion chamber. Then the turbulent flow characteristics in these engines are investigated.

METHOD FOR CALCULATING THE FLOWS IN THE INTAKE PORT AND CYLINDER

Discretization Method and Calculation Algorithm

A new calculation method has been developed for computing three-dimensional air flows in the whole region of the intake port/valve and cylinder. This method, named the GTT (Generalized Tank and Tube) method, has been created by introducing the technique of the general coordinate transformation into the finite-volume method of Gosman et al. (8) so that the body fitted non-orthogonal grids can be used.

Use is made of Cartesian coordinates (x, y, z), whose z-axis is set on the cylinder axis. The working fluid is air. In this method, basic conservation equations are discretized using the finite-volume method and general coordinate transformation. The equation representing the conservation of mass, momentum and energy of fluid in an arbitrarily shaped control volume, whose surfaces can move individually with arbitrary velocity $\vec{v}_s$, is expressed as follows:

$$\frac{d}{dt}\int\int\int_V (\rho\phi)dV + \int\int_S (\rho\phi)(\vec{v}-\vec{v}_s)\cdot\vec{n}dS - \int\int_S (\Gamma_\phi \,\mathrm{grad}\,\phi)\cdot\vec{n}dS = \int\int\int_V S_\phi dV \qquad (1)$$

where t = time, ρ = density, $\vec{v}$ = velocity vector of fluid, ϕ = each dependent variable, Γ_ϕ = effective diffusion coefficient, S_ϕ = source term, V, S = volume, surface area of a control volume, $\vec{n}$ = unit vector normal to each surface of a control volume. The terms $\mathrm{grad}\,\phi$ and $\vec{n}$ are evaluated by transforming each control volume in the physical domain (x, y, z, t) into a cube in the calculation domain, which is expressed by general curvilinear coordinates (ξ, η, ζ, τ), as shown in Fig. 1. The pressure p, density ρ and enthalpy h are allocated at the center of the control volume and the x-, y- and z-components of a velocity vector, u, v and w, are allocated at the same vertex of the control volume.

As a turbulence model, the Subgrid Scale model is applied, and the law of the wall is used as the wall-boundary conditions for velocity and temperature.

The Hybrid scheme is used for the convection term. Pressure-velocity coupling is accomplished by means of the SIMPLE algorithm. Using the fully-implicit scheme, all dependent variables are calculated iteratively at each time step; the crank angle interval is set at 2.5° or 5°. The details of the calculation method are described in Ref. (9).

Method for Generating Calculation Grids

The calculation grids for the whole domain are formed by combining the blocks of grids generated in several sub-

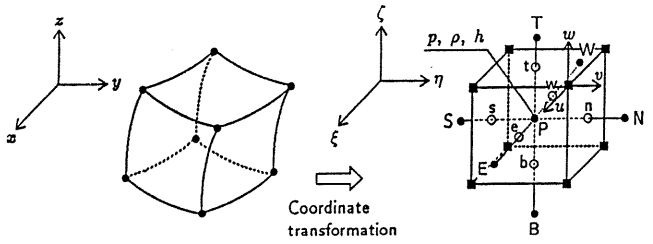

Fig. 1 Control volume

domains. Figure 2 illustrates the calculation grids for a model of single-intake valve engine (Model DC-D, to be mentioned below). As shown in Fig. 2(c), the calculation domain is composed of rectangular prisms, where the staircase-like region corresponds to the valve guide. This treatment enables the insertion of the valve stem and guide in a directed port (Fig. 2(b)). The grids for the intake port are generated algebraically using cubic splines and transfinite interpolation (10). The grids around the valve and those in the cylinder part are generated at each time step in accordance with the motion of the valve and piston using transfinite interpolation.

THE EFFECT OF INTAKE PORT CONFIGURATION ON IN-CYLINDER FLOWS IN A SINGLE-INTAKE VALVE ENGINE

Model Engine and Intake Port

The model engine is a single-intake valve engine with a disc-type combustion chamber as shown in Fig. 2(a) and (b) (bore = 130 mm, stroke = 130 mm, connecting rod length = 240 mm, compression ratio = 16.4, diameter of intake valve head = 54 mm). The valve seat angle is 45° in all models employed in this study. The intake valve moves according to the following lift curve:

$$\ell = \ell_{max} \sin^2[\pi(\Theta - \Theta_0)/\Delta\Theta] \qquad (2)$$

where ℓ_{max} = maximum valve lift (12.9 mm at Θ = 96° ATDC), Θ = crank angle measured from intake TDC, Θ_0 = -20°, $\Delta\Theta$ = 232°.

As shown in Fig. 3, three types ('normal', 'directed' and 'tangential' types) of intake ports, Models DC-N, DC-D and DC-T, are tested. Their configurations are determined with reference to Ref. (11). These ports are set tangentially in an off-center position on the cylinder head as shown in Fig. 2(a). In every model, the number of grid lines in ξ, η and ζ directions is 31x31x36 (the number of effective control volumes, i.e. fluid cells, is 17408).

Flow Characteristics during Intake Stroke

The flows in Models DC-N, DC-D and DC-T are calculated during intake stroke (from TDC to BDC) at the engine speed of 2000 rpm. At the intake port inlet, uniform velocity distribution is assumed. Figure 4 exemplifies the velocity distributions in Model DC-D. It is shown that in this model, both tumbling flow and swirl are generated at BDC. Figure 5 shows that the velocity distribution around the intake valve varies largely with crank angle; it gradually becomes non-uniform, and sufficiently non-uniform distribution is attained during about 80° - 140°ATDC. After that, the distribution gradually becomes less non-uniform. The velocity distribution around the valve is not symmetric with respect to the port axis, owing to the influence of the cylinder wall.

The swirl and tumble ratios, n_s and n_t, at BDC in the three models are shown in Fig. 6(a). Here, swirl and tumble ratios are defined as follows:

$$n_s = \Omega_s/I_s\omega_e, \quad n_t = \Omega_t/I_t\omega_e \qquad (3)$$

where ω_e = angular velocity of crank shaft rotation, Ω_s, I_s = angular momentum and inertia moment of fluid around the cylinder axis, Ω_t, I_t = angular momentum and inertia moment of fluid around an axis which is perpendicular to

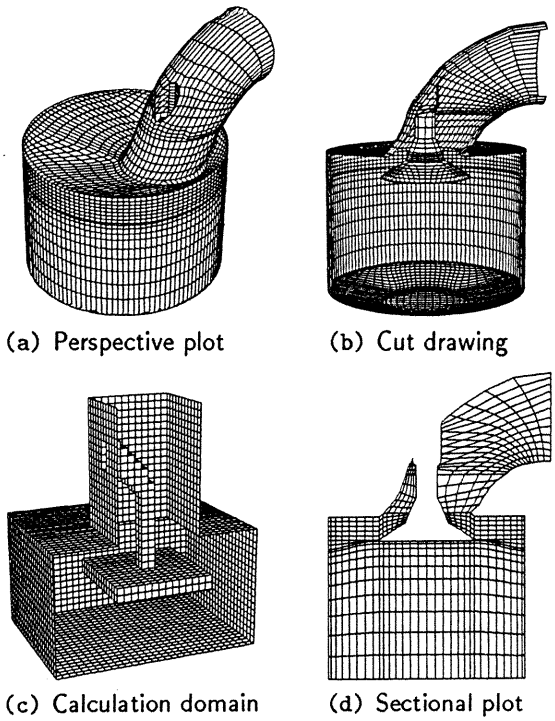

(a) Perspective plot (b) Cut drawing

(c) Calculation domain (d) Sectional plot

Fig. 2 An example of calculation grids (Model DC-D)

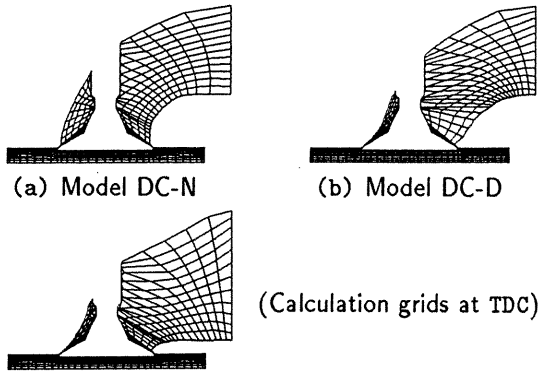

(a) Model DC-N (b) Model DC-D

(c) Model DC-T (Calculation grids at TDC)

Fig. 3 Intake ports of a single-intake valve engine

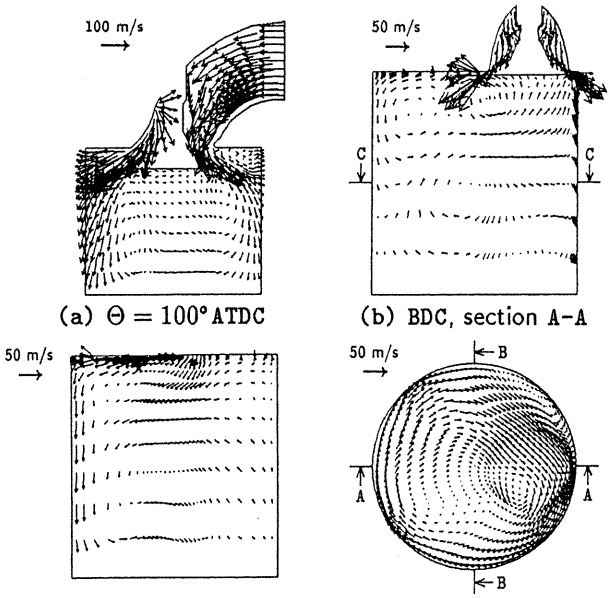

(a) Θ = 100°ATDC (b) BDC, section A-A

(c) BDC, section B-B (d) BDC, section C-C

Fig. 4 Velocity distributions in Model DC-D

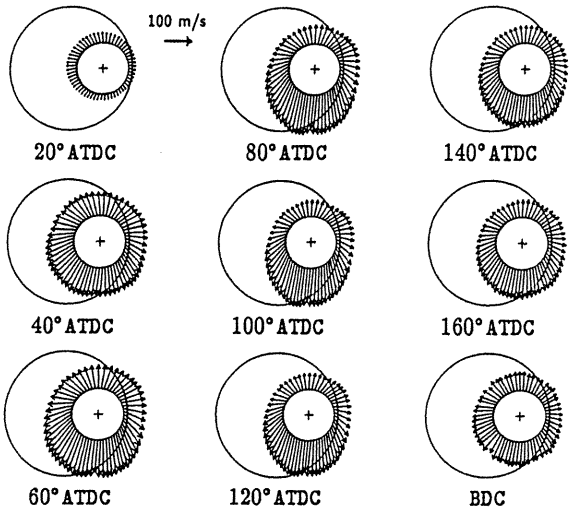

Fig. 5 Velocity distributions around the intake valve in Model DC-D

the cylinder axis and located in the middle between the cylinder head and the piston head.

Since the value of n_t varies with the azimuthal angle of the above-mentioned axis, the maximum value of n_t in each model is plotted in Fig. 6(a). It is found from this figure that Model DC-N yields only small values of n_t and n_s, while Models DC-D and DC-T yield much larger values of n_t and n_s at BDC; the latter brings about the largest values. The tendency in swirl ratios in these models is similar to the results of the steady flow experiment in Ref. (11). The velocity distributions around the valve at $\Theta = 100°$ATDC in the three models are shown in Fig. 6(b). The differences in these velocity distributions come to cause differences in n_t and n_s at BDC. A perspective view of the flow field near the valve, as shown in Fig. 7, may be useful in examining how the port configuration affects the flow around the valve.

Figure 8 shows the variations of n_s, n_t and α_t with the angle α_{port} expressing the port orientation of Model DC-D. Here, α_t denotes the azimuthal angle of the axis of tumbling motion giving maximum n_t. In the case of this port, naturally, the swirl ratio n_s varies greatly with α_{port}, while the tumble ratio n_t varies little though the angle α_t changes. It follows that when this port is set in the tangential position ($\alpha_{port} = 90°$), the strongest swirl and a tumbling flow which is as strong as in the radial position ($\alpha_{port} = 0°$) can be obtained at a time.

COMPARISON OF THE CALCULATED TURBULENCE INTENSITY OF TUMBLING FLOW WITH THE MEASURED ONE

In this and the next sections, the 'FLARE' code of the authors (12) is used. In this code, cylindrical coordinates are employed, and as a turbulence model, use is made of the $k-\varepsilon$ model with a set of standard empirical constants shown in Table 1 (k = turbulence energy, ε = dissipation rate of turbulence energy).

The tumbling flow in an engine with a centrally located shrouded intake valve, which was used by Arcoumanis et al. (13) in their experiment, is calculated during intake and compression strokes to compare the calculated turbulence intensity with the measured one. The calculated turbulence intensity $\sqrt{2k/3}$ at compression TDC on the assumption of isotropic turbulence is shown in Fig. 9 along with the experimental data (13) (v_z', v_θ' = turbulence intensity in axial and tangential directions, V_p = mean piston velocity). As the calculated values lie near the measured ones, it seems possible to investigate the turbulence generation by tumbling flow using this numerical method.

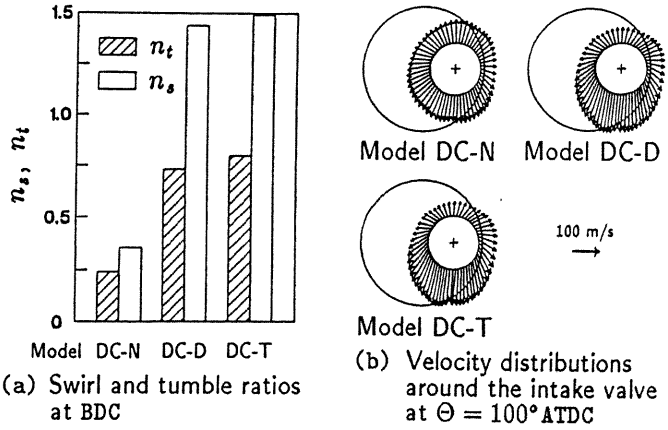

(a) Swirl and tumble ratios at BDC

(b) Velocity distributions around the intake valve at $\Theta = 100°$ATDC

Fig. 6 Flow characteristics in Models DC-N, DC-D and DC-T

Fig. 7 Perspective view of the flow field in the intake port of Model DC-D at $\Theta = 100°$ATDC

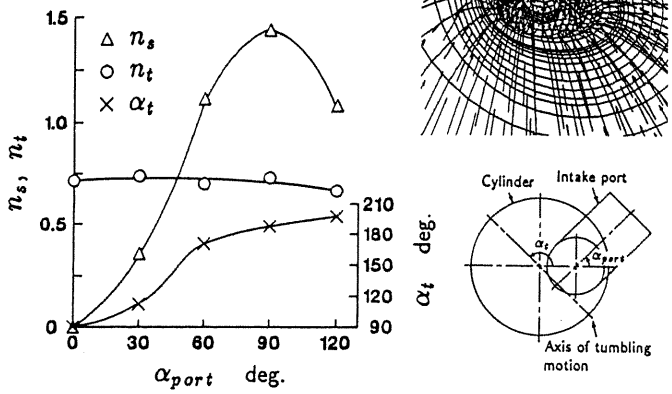

Fig. 8 Variations of the swirl and tumble ratios and α_t with the port orientation α_{port} in Model DC-D at BDC

Table 1 Coefficients for the $k-\varepsilon$ model

ϕ	Γ_ϕ	S_ϕ
k	μ_{eff}/σ_k	$G-\rho\varepsilon$
ε	$\mu_{eff}/\sigma_\varepsilon$	$\frac{\varepsilon}{k}(C_1G-C_2\rho\varepsilon)+C_3\rho\varepsilon\mathrm{div}\,\vec{v}$

$\mu_{turb} = C_\mu\rho k^2/\varepsilon$, $C_\mu = 0.09$, $\sigma_k = 1.0$, $\sigma_\varepsilon = 1.3$
$C_1 = 1.44$, $C_2 = 1.92$, $C_3 = -0.373$

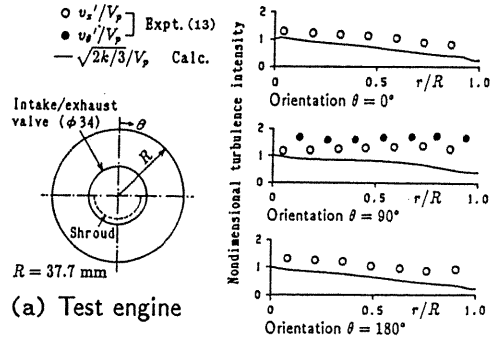

(a) Test engine

(b) Radial distributions of turbulence intensity at compression TDC

Fig. 9 Comparison of the calculated turbulence intensity with the measured one (13) in an engine with a shrouded valve

FLOW CHARACTERISTICS IN A DUAL-INTAKE VALVE ENGINE WITH A DISC-TYPE COMBUSTION CHAMBER

Model Engine and Inflow Velocity Distributions

The model engine, which was employed in a previous work (12), is a dual-intake valve engine with a disc-type combustion chamber (bore = 130 mm, stroke = 150 mm, connecting rod length = 260 mm, compression ratio = 8.5, diameter of each intake valve = 44 mm). In this model, intake ports are not included in the calculation domain for simplicity, but various velocity distributions ('normal' and 'directed' port types) are prescribed around the intake valves. The velocity distributions given around the valves are shown in Fig. 10, where N_0 = ratio of the maximum velocity to the minimum velocity, and β = angle between the maximum velocity direction and the radial direction. For simplicity, the profiles of these velocity distributions are kept unchanged regardless of crank angle.

Flow Characteristics during Intake and Compression Strokes

The in-cylinder flows are calculated from intake TDC to compression TDC at 1200 rpm. The turbulence energy k is calculated using the $k-\varepsilon$ model; as the inlet boundary condition for k, the relative turbulence intensity at the valve periphery is set at 15 %. Figures 11 and 12 show the temporal variations of the spatially averaged kinetic energy of mean flow, E_m, and the spatially averaged turbulence energy, k_m, during intake and compression strokes. Also shown in Fig. 12(b) is the spatially averaged turbulence energy k_m in the case where a solid-body swirl (initial swirl ratio = 2) without any vertical vortex component is given at BDC (Model DC-SBS); the initial values of k and ε are equated to those at BDC in Model DC-DD5. The tumble ratio n_t and swirl ratio n_s at intake BDC in each model are shown in Fig. 13. The values of k_m at intake BDC and compression TDC in each model are shown in Fig. 14, where the values of k_m are normalized by those in Model DC-NN.

Figures 11(a) and 12(a) show that during intake stroke, the values of E_m and k_m in every model initially increase very largely, but after reaching the maximum values they decrease to small values. It is found that the values of k_m at BDC in all models differ little from one another (Fig. 12(b)),though the differences in the values of E_m at BDC are large between the models (Fig. 11(b)). From Fig. 12(b), the following is observed:

In every model, the turbulence energy k_m decreases rapidly in the first half of compression stroke; this decrease is especially large in Model DC-SBS. In the second half of compression stroke, k_m in each model except Model DC-SBS increases considerably at first, and then it finally decreases. This increase in k_m is very large in Model DC-DD5; this is probably due to its having the largest tumble ratio (Fig. 13). Consequently, Model DC-DD5 yields the largest turbulence energy at compression TDC (Fig. 14). In Model DC-SBS, on the contrary, k_m is the smallest throughout the compression stroke except at the beginning. When comparing the value of k_m near compression TDC in Model DC-DD3S with that in Model DC-DD3 (Fig. 12(b)), k_m in Model DC-DD3S is only a little smaller than that in Model DC-DD3 in spite of the much smaller tumble ratio found in Model DC-DD3S (Fig. 13). This is probably because Model DC-DD3S includes a swirl component (Fig. 13), i.e. the in-cylinder flow is in the state of inclined swirl. Such behavior of k_m in tumbling flow and inclined swirl is similar to the experimental result (5).

As shown in Fig. 11(b), the kinetic energy of mean flow E_m near compression TDC in Model DC-DD3S, i.e. in the case of inclined swirl, is much larger than those in the other models, i.e. in the case of tumbling flow. It is inferred, therefore, that the inclined swirl may be effective for promoting combustion if its large kinetic energy near compression TDC could be used for enhancing the turbulence by devising the combustion chamber shape, as mentioned in Ref. (5).

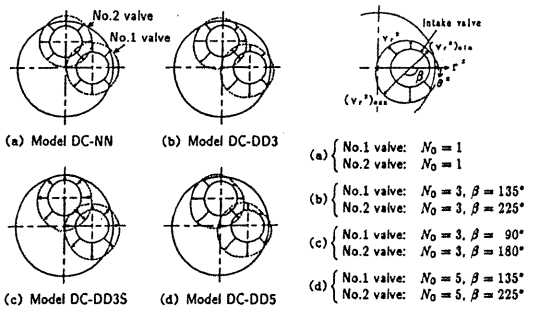

Fig. 10 Velocity distributions around the intake valves in a dual-intake valve engine with a disc-type combustion chamber

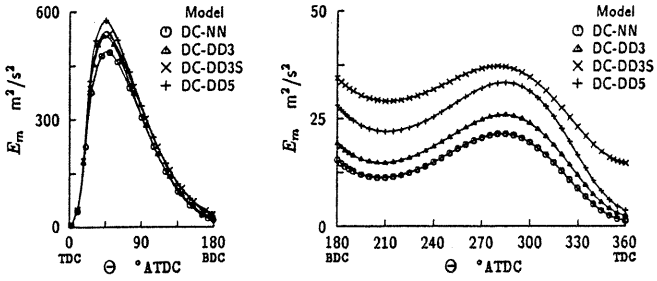

(a) Intake stroke (b) Compression stroke

Fig. 11 Spatially averaged kinetic energy of mean flow

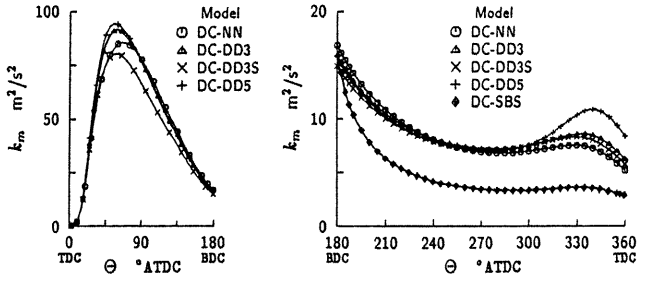

(a) Intake stroke (b) Compression stroke

Fig. 12 Spatially averaged turbulence energy

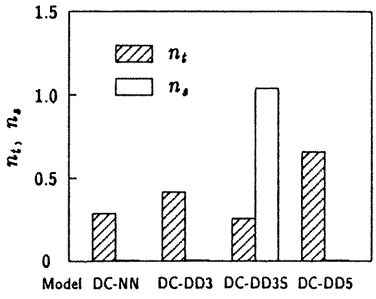

Fig. 13 Tumble and swirl ratios at intake BDC

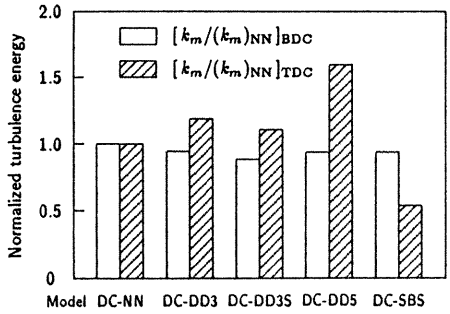

Fig. 14 Normalized turbulence energy at intake BDC and compression TDC

FLOW CHARACTERISTICS IN A DUAL-INTAKE VALVE ENGINE WITH A PENTROOF-TYPE COMBUSTION CHAMBER

Model Engine and Intake Port

The model engine is a dual-intake valve engine with a pentroof combustion chamber as shown in Fig. 15(a) (bore = 78 mm, stroke = 69.7 mm, connecting rod length = 121.5 mm, compression ratio = 9.5, TDC clearance height = 1.2 mm). This engine is equipped with two separate intake ports of the same configuration and two intake valves of the same size (valve head diameter = 30 mm). Both valves move according to Eq. (2), where ℓ_{max} = 7.17 mm, $\Theta_0 = -20°$ and $\Delta\Theta = 232°$). Engine speed is set at 2000 rpm.

Two types ('normal' and 'directed' types) of intake ports, Models PR-NN (Fig. 15(c)) and PR-DD (Fig. 15(d)), are tested. These ports are designed on the basis of Models DC-N and DC-D (Fig. 3(a) and (b)). The calculation grids for intake stroke are shown in Fig. 16 (the number of grid lines in ξ, η and ζ directions is 41x41x35, and the number of effective control volumes is 29336). When the flows during compression stroke are calculated, the intake ports and valves are removed as shown in Fig. 15(b) (the number of grid lines in ξ, η and ζ directions is 31x31x21, and the number of effective control volumes is 15840).

Flow Characteristics during Intake Stroke

The flows during intake stroke (from TDC to BDC) are calculated using the Subgrid Scale model as a turbulence model for saving computation time. At each port inlet, uniform velocity distribution is assumed. The calculated velocity fields at $\Theta = 100°$ATDC (near the time of maximum valve lift) and at BDC are shown in Figs. 17 and 18. Close observation of these figures reveals that in these two models, the in-cylinder flow patterns in each section which holds the port axis are considerably different from each other; at $\Theta = 100°$ATDC, differences in the development of two vertical vortices rotating in opposite directions exist between the two models. At BDC in Model PR-DD, one large vertical vortex, i.e. tumbling flow, and one small vertical vortex are brought about because of the non-uniform velocity distributions around the valves. In Model PR-NN, however, twin vertical vortices are generated at BDC because of the less non-uniform velocity distributions around the valves. Comparing the velocity distributions around the intake valves in Model PR-DD (Fig. 18(a)) with those in Model DC-D (Fig. 5), the port configuration of Model PR-DD is still open to modification for obtaining stronger tumbling flow.

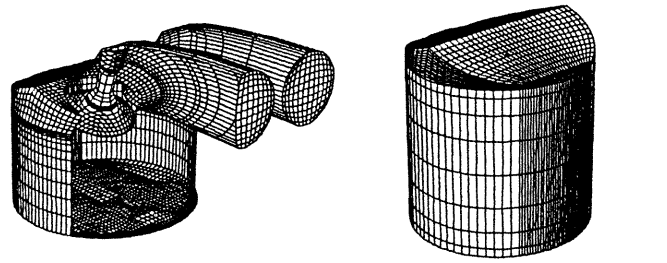

(a) Model for intake stroke (Model PR-DD)

(b) Model for compression stroke (Models PR-NN/DD)

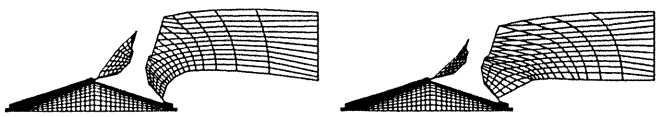

(c) Intake port of Model PR-NN

(d) Intake port of Model PR-DD

(Calculation grids at TDC)

Fig. 15 Dual-intake valve engine with a pentroof-type combustion chamber

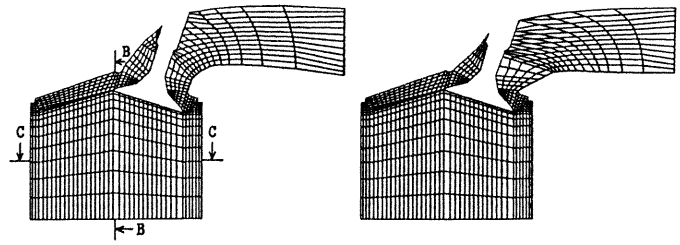

(a) Model PR-NN (section A-A)

(b) Model PR-DD (section A-A)

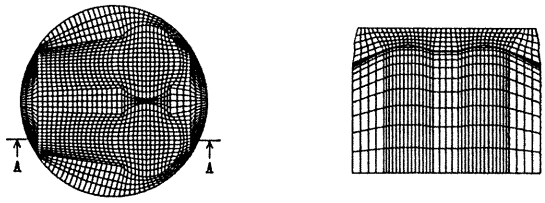

(c) Models PR-NN/DD (section C-C)

(d) Models PR-NN/DD (section B-B)

Fig. 16 Calculation grids for Models PR-NN and PR-DD (for intake stroke)

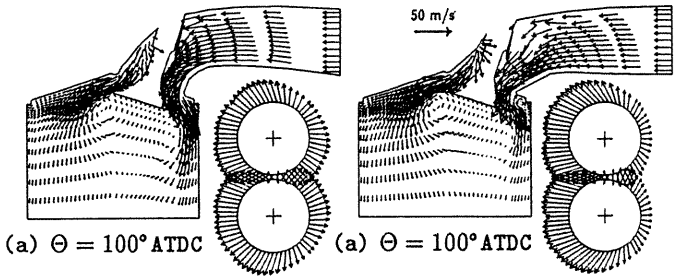

(a) $\Theta = 100°$ATDC

(a) $\Theta = 100°$ATDC

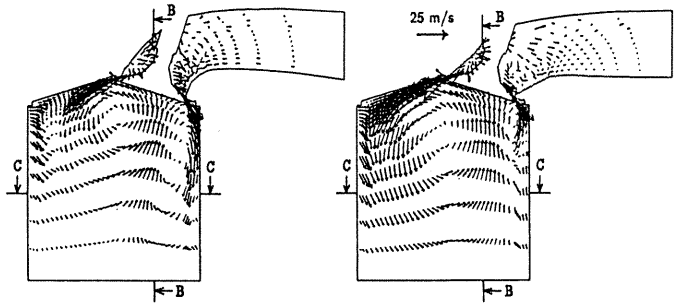

(b) BDC (section A-A)

(b) BDC (section A-A)

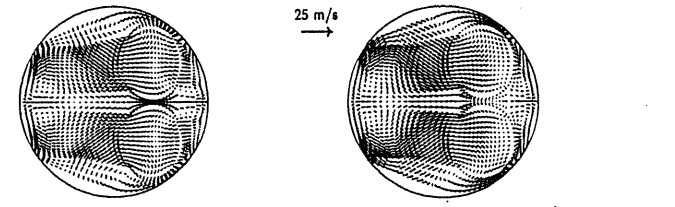

(c) BDC (section C-C)

(c) BDC (section C-C)

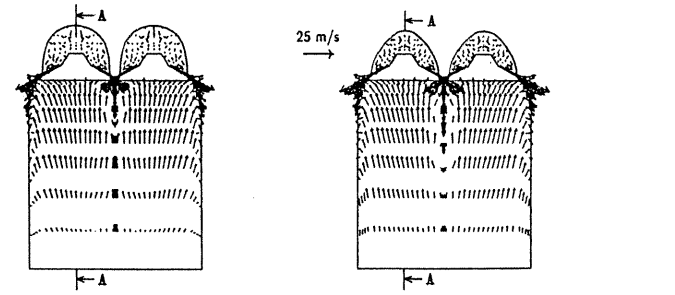

(d) BDC (section B-B)

(d) BDC (section B-B)

Fig. 17 Velocity distributions in Model PR-NN during intake stroke

Fig. 18 Velocity distributions in Model PR-DD during intake stroke

Flow Characteristics during Compression Stroke

The velocity fields at intake BDC are interpolated to obtain the initial velocity fields for calculating the flows during compression stroke. In this calculation, the $k-\varepsilon$ model (Table 1) is used as a turbulence model. As the turbulence energy k and dissipation rate ε at BDC, the spatially averaged values of k and ε at BDC in Model DC-DD5 (Fig. 10(d)) are tentatively used for both Models PR-NN and PR-DD. The distributions of the calculated velocity and turbulence energy are shown in Figs. 19 and 20. In Model PR-DD, tumbling flow survives throughout compression stroke, while in Model PR-NN, twin vortices remain. As shown in Fig. 21, during compression stroke, the tumble ratio n_t in Model PR-DD is much higher than that in Model PR-NN except near compression TDC. In Model PR-NN, non-zero values of n_t during compression stroke mean that twin vertical vortices are not symmetric. The temporal variation of the spatially averaged turbulence energy k_m in each model is shown in Fig. 22. Also shown in this figure is the turbulence energy k_m in the case where a solid-body swirl (initial swirl ratio = 2) without any vertical vortex component is given at BDC (Model PR-SBS). In every model, the turbulence energy k_m decreases rapidly in the first half of compression stroke. After that, in Models PR-NN and PR-SBS, k_m increases a little and then finally decreases. In Model PR-DD, however, k_m increases considerably before it finally decreases. This model, therefore, yields the largest turbulence energy near compression TDC. On the contrary, k_m in Model PR-SBS is the smallest throughout the compression stroke. In the first half of compression stroke, the value of k_m in Model PR-NN is only a little smaller than that in Model PR-DD. This means that even twin vertical vortices are effective for suppressing the decay of turbulence. As a result, it has been found that, as is the case of the tumbling flow in the disc-type combustion chamber, the tumbling flow can generate much stronger turbulence in the pentroof-type combustion chamber than can the solid-body swirl.

As to CPU time, calculation of the flow in Model PR-DD, for example, took about 120 minutes for the intake stroke and about 110 minutes for the compression stroke on FACOM VP-200.

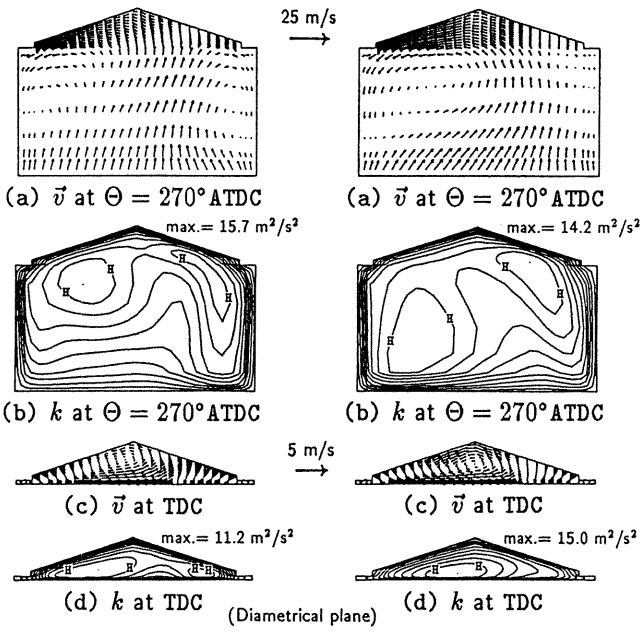

Fig. 19 Velocity and turbulence energy distributions in Model PR-NN during compression stroke

Fig. 20 Velocity and turbulence energy distributions in Model PR-DD during compression stroke

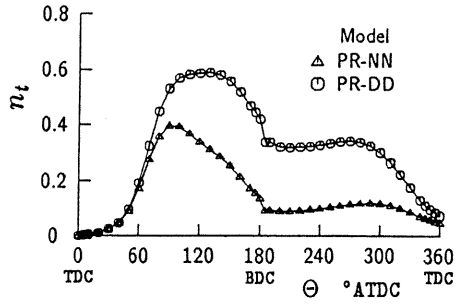

Fig. 21 Variation of tumble ratio with crank angle

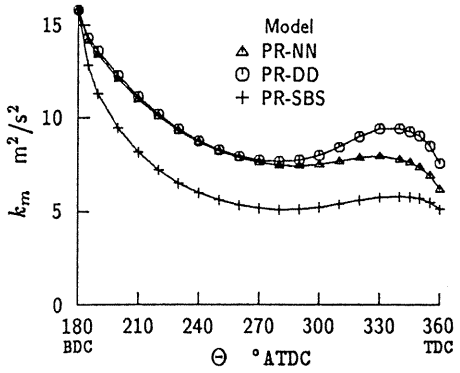

Fig. 22 Variation of spatially averaged turbulence energy with crank angle

CONCLUSIONS

The flows in the whole region of the intake port and cylinder, including the moving intake valve with a stem, in single- and dual-intake valve engines have been successfully calculated using the GTT method. In a single-intake valve engine, the variations of the tumble and swirl components at intake BDC with the configuration and orientation of intake port have been demonstrated. It has been found that in dual-intake valve engines, the tumbling flow generates much stronger turbulence near compression TDC in both disc-type and pentroof-type combustion chambers than does the horizontal solid-body swirl. It is inferred that the inclined swirl may be effective for promoting combustion if its large kinetic energy near compression TDC could be converted into turbulence energy.

ACKNOWLEDGMENT

This work has been partially supported by a Grant-in-Aid for Scientific Research (Priority Areas to Combustion Mechanism) from the Ministry of Education, Science and Culture of Japan.

REFERENCES

1. Kyriakides, S. C. et al., Proc. IMechE, 1988-3 (1988), 195.
2. Yamada, T. et al., Proc. JSAE, No. 882 (1988), 367 (in Japanese).
3. Le Coz, J-F. et al., SAE Paper 900056 (1990).
4. Khalighi, B., SAE Paper 900059 (1990).
5. Arcoumanis, C. et al., SAE Paper 900060 (1990).
6. Naitoh, K. et al., SAE Paper 900256 (1990).
7. Haworth, D. C. et al., SAE Paper 900257 (1990).
8. Gosman, A. D. et al., TEACH-T, Mech. Engrg. Dept. Report, Imperial College of Sci. and Tech., (1976).
9. Wakisaka, T. et al., Proc. 8th Joint Symp. on Internal Combustion Engines (1990), 231 (in Japanese).
10. Eriksson, L. E., AIAA J., Vol. 20, No. 10 (1982), 1313.
11. Fitzgeorge, D. et al., Proc. IMechE, Vol. 177, No. 4 (1963), 151.
12. Wakisaka, T. et al., Proc. IMechE, 1988-3 (1988), 73.
13. Arcoumanis, C. et al., SAE Paper 841360 (1984).